

# Compressive Sensing Based High-Resolution Polarimetric Through-the-Wall Radar Imaging Exploiting Target Characteristics

Qisong Wu, *Member, IEEE*, Yimin D. Zhang, *Senior Member, IEEE*, Fauzia Ahmad, *Senior Member, IEEE*, and Moeness G. Amin, *Fellow, IEEE*

**Abstract**—In this letter, we consider high-resolution through-the-wall radar imaging (TWRI) using compressive sensing (CS) techniques that exploit the target and sensing characteristics. Many TWRI problems can be cast as inverse scattering involving few targets and, thus, benefit from CS and sparse reconstruction techniques. In particular, recognizing that most indoor targets are spatially extended, we exploit the clustering property of the sparse scene to achieve enhanced imaging capability. In addition, multiple polarization sensing modalities are used to obtain increased observation dimensionality within the group sparsity framework. The recently developed cluster multi-task Bayesian CS approach is modified to effectively solve the formulated group and clustered sparse problem. Experimental results are presented to demonstrate the superiority of the proposed approach.

**Index Terms**—Through-the-wall radar imaging, compressive sensing, group sparsity, cluster structure

## I. INTRODUCTION

Through-the-wall radar imaging (TWRI) has attracted great attention in the last decade and has found a variety of important civil and military applications [1]. A number of techniques have been developed to achieve high-quality imaging of targets behind walls, examples being wall parameter estimation, wall clutter mitigation, wideband imaging, and multipath exploitation. Often and in many TWRI applications, however, the behind-the-wall scene being investigated contains few targets of interest, i.e., a large portion of the space is unoccupied, thereby rendering the scene as sparse. In this case, TWRI can be effectively performed by taking advantage of the recent advances in compressive sensing (CS) and sparse reconstruction techniques [2].

In TWRI applications, both system and target characteristics can be utilized for improved sparse imaging. For example, recognizing that most indoor targets are spatially extended, the clustering property can be exploited to achieve enhanced imaging capability. In addition, multiple polarization sensing can be used to obtain increased observation dimensionality within the group sparsity framework. In group sparsity, the nonzero scattering coefficients have a common support for different polarizations, but their exact values may differ. The aforementioned properties have been separately considered in the context of TWRI to improve the sparse reconstruction performance, leading to higher imaging resolution, clutter reduction, and target separability [3]–[5].

Group sparse problems can be solved by a number of existing algorithms, such as block orthogonal matching pursuit (BOMP) [6] and group Lasso (gLasso) [7]. The multi-task CS

(mt-CS) algorithm [8] generally provides improved solutions as compared to other methods in solving a large class of real-valued group sparse problems, and the complex-valued signals are considered in [9]–[12]. On the other hand, spatially extended targets can be considered as clustered or structured sparse signals, which can be reconstructed using, e.g., overlapping group sparse (GS) reconstruction [13], Bayesian group-sparse modeling based on variational inference (GS-VB) [14], and CluSS-MCMC [15]. The recently developed clustered multi-task Bayesian CS (CMT-BCS) [16] treats both group sparsity and clustering sparsity in a unified framework.

In this letter, we exploit both group sparsity, stemming from the multi-polarization sensing modality, and clustering sparsity, due to the targets' spatial extent, to achieve high-resolution sparse TWRI. The scene reconstruction is formulated as a clustered group sparse problem. To solve such a problem, we modify the recently proposed CMT-BCS algorithm [16] from real-valued formulations to accommodate complex-valued sparse signals and from handling a one-dimensional (1-D) signal to a two-dimensional (2-D) image scene. As such, improved target imaging capability is achieved even when employing a thinned array aperture and a reduced number of frequency observations. Note that conventional inverse scattering approaches suffer under such reduced observations in spatial and frequency domains. Supporting results using real data measurements are provided to demonstrate the superiority of the proposed approach.

*Notation:* We use lower-case (upper-case) bold characters to denote vectors (matrices). In particular,  $\mathbf{I}_N$  denotes the  $N \times N$  identity matrix. Superscript  $(\cdot)^H$  denotes the conjugate transpose, and  $\circ$  denotes element-wise multiplication.  $p(\cdot)$  represents the probability density function (pdf), whereas  $p(\cdot|—)$  denotes the conditional pdf given other variables.  $\mathcal{CN}(x|a, b)$  denotes a complex Gaussian random variable  $x$  with mean  $a$  and variance  $b$ , and  $\text{Gamma}(x|a, b)$  means that  $x$  follows a Gamma distribution with parameters  $a$  and  $b$ .  $\text{Bern}(x|\pi)$  denotes that  $x$  follows a Bernoulli distribution with weight  $\pi$ , whereas  $\text{Beta}(x|a, b)$  means  $x$  to follow a beta distribution with weights  $a$  and  $b$ .  $\delta(x)$  represents the delta function of  $x$ .

## II. SCATTERING MODEL

We consider a three-dimensional (3-D) scattering experiment with a synthetic mono-static 2-D antenna array. The transmitting antenna radiates both  $x$ - and  $y$ -polarized fields within the frequency band  $f \in [f_{\min}, f_{\max}]$ , collects the scattered field at the same location, and then moves to the next location of the synthetic aperture  $D_O = [-x_{\text{Max}}, x_{\text{Max}}] \times [y_{\text{Min}}, y_{\text{Max}}]$ . The synthetic array aperture has an extent of  $2x_{\text{Max}}$  and  $(y_{\text{Max}} - y_{\text{Min}})$  along the  $x$ - and  $y$ -axes, respectively.

This work is supported in part by the Army Research Office and the Army Research Laboratory under contract W911NF-11-1-0536. The authors are with the Center for Advanced Communications, Villanova University, Villanova, PA 19085, USA.

The scene under surveillance is located within the investigation domain of  $D_S = [-a, a] \times [0, h] \times [z_{\min}, z_{\min} + b]$  embedded in a known background medium. Here,  $2a$  is the width,  $h$  is the height, and  $b$  is the range depth of the investigation domain. We consider multiple polarization modes, e.g., vertical-vertical (VV) and horizontal-horizontal (HH). Denote the number of polarization modes being used by  $L$ . As such, the observation configuration operates in a “multiple mono-static sensors with multi-polarization” reflection mode.

For high-contrast scatterers, the Kirchhoff approximation can be exploited to obtain a linearized scattering equation [17]

$$s_l(x_O, y_O, k_0) = \iint_{D_S} G_l(x_O, y_O, x, y, z, k_0) \cdot E_l(x_O, y_O, x, y, z, k_0) w_l(x, y, z) dx dy dz, \quad (1)$$

where  $s_l(x_O, y_O, k_0)$  is the scattered field collected at the observation position  $[x_O, y_O] \in D_O$  for polarization  $l \in [1, \dots, L]$ ,  $k_0$  is the wavenumber,  $G(x_O, y_O, x, y, z, k_0)$  represents the 3-D Green’s function which relates the wave propagation process from the transmitter to the target and then back to the receiver [18],  $E_l(x_O, y_O, x, y, z, k_0)$  is the field impinging on the target located at  $(x, y, z) \in D_S$ , and  $w(x, y, z)$  represents the unknown target scattering coefficient to be estimated. Accordingly, the objective of the TWRI problem is to solve (1) for  $w(x, y, z), \forall (x, y, z) \in D_S$ . As is well known, this type of inverse scattering problem is ill-posed [19]. A commonly used approach is the back-projection technique, which exhibits poor resolution and high side lobes when a limited and thinned array aperture is employed. However, often and in many TWRI applications, the scene is sparse, thereby permitting the scene reconstruction to be cast as an inverse scattering problem involving few targets and can be solved by using CS and sparse reconstruction approaches.

Toward this end, the problem in (1) first needs to be discretized. We consider availability of observations from  $N$  synthetic array positions  $[x_{On}, y_{On}] \in D_O, n = 1, \dots, N$ , for each polarization, and stack them into an  $N \times 1$  vector  $\mathbf{y}_l$ . The observation scene is discretized by suitably choosing a grid of  $M$  pixels, with the scattering coefficient corresponding to polarization  $l$  at pixel  $(x, y, z) \in D_S$  represented by  $w_l(x, y, z)$ . Stack  $w_l(x, y, z)$  corresponding to all the pixels into a vector  $\mathbf{w}_l$ . Note that  $\mathbf{w}_l$  exhibits group sparsity across all polarization modes, i.e.,  $\mathbf{w}_1, \dots, \mathbf{w}_L$  share a common sparsity support, but the exact values may vary with polarization. Furthermore, assuming that the observations are made at  $K$  frequencies, i.e.,  $f_m \in [k_{0\min}, k_{0\max}], m = 1, \dots, K$ , they yield  $K$  corresponding wavenumbers  $k_{0m}, m = 1, \dots, K$ . Therefore, the discretized counterpart of (1) is given by

$$\mathbf{y}_l = \mathbf{A}_l \mathbf{w}_l, \quad l \in [1, \dots, L], \quad (2)$$

where  $\mathbf{A}_l \in \mathcal{C}^{KN \times M}$  is the sensing matrix, which accounts for the contribution of the Green’s function and the impinging field for polarization  $l$ .

### III. CLUSTERED MULTI-TASK BAYESIAN COMPRESSIVE SENSING BASED SCENE RECONSTRUCTION

Within the CS framework, we, in essence, aim at acquiring a good quality scene reconstruction using only a subset of

the full measurements. A number of measurement schemes have been proposed for reduction of the acquired data volume [2], [20]. The common feature of these schemes is that they can simply be expressed as a measurement or downsampling matrix  $\mathbf{D} \in \mathcal{C}^{J \times KN}$  acting on the full measurement  $\mathbf{y}_l$ , where  $J \ll KN$  is the number of reduced measurements. For stepped-frequency operation, a binary measurement matrix  $\mathbf{D} \in [0, 1]^{J \times KN}$  is a reasonable choice [3], [20]. Using (2) and the measurement matrix  $\mathbf{D}$ , we can express an undersampled measurement vector  $\mathbf{s}_l \in \mathcal{C}^J$  as

$$\mathbf{s}_l = \mathbf{D} \mathbf{y}_l = \Phi_l \mathbf{w}_l + \epsilon_l, \quad (3)$$

where  $\Phi_l = \mathbf{D} \mathbf{A}_l$  is the dictionary matrix for polarization  $l$  and, without loss of generality, an additive noise vector  $\epsilon_l$  is considered. Having arrived at the reduced data model in (3), a clustered multi-task reconstruction problem is formulated and solved in the Bayesian CS framework.

We place a spike-and-slab prior on the scattering coefficients  $\mathbf{w}_l$  to enforce group sparsity across all polarization modes,

$$p(\mathbf{w}_l | \boldsymbol{\pi}, \boldsymbol{\beta}) = \prod_{i=1}^M [(1 - \pi_i) \delta(w_{il}) + \pi_i \mathcal{CN}(w_{il} | 0, \beta_i^{-1})], \quad (4)$$

where  $\beta_i$  is the precision (reciprocal of the variance) of the Gaussian distribution and  $\pi_i$  is the prior probability of a nonzero element in the  $i$ th pixel, i.e., a large weight  $\pi_i$  corresponds to a high probability that the entry takes a nonzero value, whereas a small  $\pi_i$  tends to generate a zero entry. As  $\pi_i$  is shared across all polarization modes, the corresponding prior is capable of encouraging group sparsity in the underlying hierarchical Bayesian CS (BCS) framework. Note that the above expression is extended to complex Gaussian distributions from the real-valued model as in [16] to handle the underlying complex-valued TWRI problem.

To make the inference analytical, we introduce two latent random variables,  $\boldsymbol{\theta}_l$  and  $\mathbf{z}$ , which respectively follow complex-valued Gaussian and Bernoulli distributions. Their element-wise product,  $\boldsymbol{\theta}_l \circ \mathbf{z}$ , follows the pdf in (4), i.e.,

$$p(\boldsymbol{\theta}_l, \mathbf{z}) = \prod_{i=1}^M [\mathcal{CN}(\theta_{il} | 0, \beta_i^{-1})]^{z_i} \text{Bern}(z_i | \pi_i). \quad (5)$$

In this case, the group sparsity is characterized by the same  $z_i$  for the  $i$ th position across the  $L$  polarization modes. On the other hand, scattering coefficients in the  $i$ th group  $\boldsymbol{\theta}_i = [\theta_{i1}, \dots, \theta_{iL}]$ , in general, take different values.

To acquire the trackable posterior of  $\beta_i$ , we place a Gamma prior, which is the conjugate to the Gaussian distribution, on  $\beta_i$ , i.e.,  $\beta_i \sim \text{Gamma}(a, b), i \in [1, \dots, M]$ , where  $a$  and  $b$  are hyper-parameters. A Gaussian prior is placed on the additive noise as  $\epsilon_l \sim \mathcal{CN}(\epsilon_l | \mathbf{0}, \alpha_l^{-1} \mathbf{I}_N)$ . In a similar manner, a Gamma prior is placed on  $\alpha_l$  to acquire an analytical posterior distribution, i.e.,  $\alpha_l \sim \text{Gamma}(c, d), l \in [1, \dots, L]$ , where  $c$  and  $d$  are hyper-parameters.

To incorporate the dependency structure among pixels, the cluster pattern was considered in [15], [16] for the 1-D case involving two neighboring pixels. Three-level cluster patterns, i.e., Strong Rejection, Weak Rejection, and Strong Acceptance, were designed according to the number of neighboring pixels,

denoted as  $\kappa_i$ . To facilitate the inference, a Beta prior, which is conjugate to the Bernoulli distribution, with different sets of parameters  $\{e_i, f_i\}$ , where  $i \in [0, 1, 2]$  for the three patterns, was placed on weights  $\pi_i$  according to the cluster patterns.

In the underlying TWRI problem, we generalize the approach to accommodate the 2-D imaging scene which involves a higher number of neighboring pixels. In this case, the values of  $\{e_i, f_i\}$  are determined through nonlinear functions of  $\kappa_i$ . More specifically,  $e_i$  increases monotonically with  $\kappa_i$ , whereas  $f_i$  is a monotonically decreasing function of  $\kappa_i$ . Therefore, for small values of  $\kappa_i$ ,  $e_i \ll f_i$ , yielding a strong rejection of the pixel under test, whereas for a large value of  $\kappa_i$ ,  $e_i \gg f_i$ , which implies a strong acceptance of the pixel.

Fig. 1 shows some examples of these patterns. In particular, Fig. 1(a) shows a strong rejection pattern where all of neighboring pixels are zero ( $\kappa_i = 0$ ), whereas Fig. 1(b) shows a weak rejection pattern where one of neighboring pixels is nonzero ( $\kappa_i = 1$ ). Fig. 1(c) shows a strong acceptance pattern with all nonzero neighboring pixels ( $\kappa_i = 8$ ). This yields a generalized CMT-BCS with complex-valued sparse entries.

We use a Gibbs sampler to implement the Bayesian inference. For convenience, we define the collection of hyperparameters as  $\Xi \triangleq \{a, b, c, d, \mathbf{e}, \mathbf{f}\}$  with  $\mathbf{e} \triangleq \{e_0, e_1, \dots, e_{B-1}\}$  and  $\mathbf{f} \triangleq \{f_0, f_1, \dots, f_{B-1}\}$ , while the collection of random variables is defined as  $\Theta \triangleq \{\boldsymbol{\theta}, \mathbf{z}, \boldsymbol{\pi}, \boldsymbol{\alpha}, \boldsymbol{\beta}\}$ . We also form a matrix from the observed data corresponding to the  $L$  polarizations as  $\mathbf{Y} = \{\mathbf{y}_1, \dots, \mathbf{y}_L\}$  and  $\boldsymbol{\Psi} = \{\boldsymbol{\Phi}_1, \dots, \boldsymbol{\Phi}_L\}$ . Then, the explicit form of the full likelihood based on the generative model is expressed as

$$p(\mathbf{Y}, \boldsymbol{\Psi}, \Theta | \Xi) = \prod_{l=1}^L \mathcal{CN}(\mathbf{y}_l | \boldsymbol{\Phi}_l(\boldsymbol{\theta}_l \circ \mathbf{z}), \alpha_l^{-1} \mathbf{I}_N) \text{Bern}(z_i | \pi_i) \cdot \prod_{l=1}^L \prod_{i=1}^M [\mathcal{CN}(\theta_{il} | 0, \beta_i^{-1})]^{z_i} \text{Gamma}(\alpha_l | c, d) \cdot \prod_{i=1}^M \text{Beta}(\pi_i | \mathbf{e}, \mathbf{f}, \mathbf{z}_{\eta_i}) \text{Gamma}(\beta_i | a, b). \quad (6)$$

Utilizing the conjugate properties of the complex Gaussian and Gamma distributions, the Beta and Bernoulli distributions, we analytically acquire the respective posterior distributions for each random variable  $\{\mathbf{z}, \boldsymbol{\theta}, \boldsymbol{\pi}, \boldsymbol{\alpha}, \boldsymbol{\beta}\}$ .

The posterior probability of  $z_i = 1$  given other variables is acquired analytically by utilizing the logistic function as,

$$p(z_i = 1 | -) = (1 + e^{-u})^{-1}, \quad (7)$$

where

$$u = \frac{1}{2} \sum_{l=1}^L \left( \log(\beta_i \sigma_{il}) + \sigma_{il} \alpha_l^2 \mathbf{y}_{\setminus il}^H \boldsymbol{\phi}_i \boldsymbol{\phi}_i^H \mathbf{y}_{\setminus il} \right) + \log \frac{\pi_i}{1 - \pi_i},$$

$\sigma_{il} = (\alpha_l \boldsymbol{\phi}_{il}^H \boldsymbol{\phi}_{il} + \beta_i)^{-1}$ ,  $\mathbf{y}_{\setminus il} = \mathbf{y}_l - \sum_{k \neq i} \boldsymbol{\phi}_{kl} z_k \theta_{kl}$ , and  $\boldsymbol{\phi}_{il}$  is the  $i$ th column of the measurement matrix  $\boldsymbol{\Phi}_l$ .

For  $z_i = 1$ , the posterior distribution of  $\theta_{il}$  is given by,

$$p(\theta_{il} | -) = \mathcal{CN}(\theta_{il} | \sigma_{il} \alpha_l \boldsymbol{\phi}_{il}^H \mathbf{y}_{\setminus il}, \sigma_{il}). \quad (8)$$

For  $z_i = 0$ , the value of variable  $\theta_{il}$  is drawn from its prior. Once the  $\boldsymbol{\theta}_l$  and  $\mathbf{z}$  are estimated, the corresponding scattering

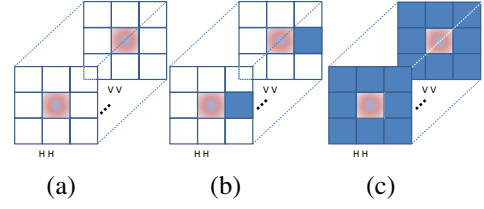


Fig. 1. Examples of clustering patterns for a 2-D image. (a) a strong rejection example with  $\kappa_i = 0$ ; (b) a weak rejection example with  $\kappa_i = 1$ ; and (c) a strong acceptance example with  $\kappa_i = 8$ .

coefficients  $\mathbf{w}$  are obtained. We refer to [16] for details on the update formulas of the other random variables  $\{\boldsymbol{\pi}, \boldsymbol{\beta}, \boldsymbol{\alpha}\}$ .

Since the inference of model parameters is implemented by the Gibbs sampler, it inherently requires sequential sampling. The computation complexity of the proposed algorithm is  $\mathcal{O}(J^3 \times L \times M \times N_{\text{maxiter}})$ , where  $N_{\text{maxiter}}$  is the maximum number of iterations. It is higher than fast greedy based BCS approaches and both the GS-VS and the BSBL algorithms based on dimension reduction operation, because the proposed method needs to go through all  $L \times M$  elements in each MCMC iteration.

#### IV. EXPERIMENT RESULTS

A TRWI experiment was carried out in the Radar Imaging Lab, Villanova University. The 2-D antenna array aperture was synthesized using the Damaskos Field Probe Scanner model 7X7Y, shown in Fig. 2(a). The Port 1 antenna of Fig. 2(a) was oriented for the horizontal polarization whereas the Port 2 antenna was oriented for the vertical polarization. The scan area was configured to allow both Port 1 and 2 antennas to scan a zone of  $1.2\text{m} \times 1.2\text{m} = 1.24\text{m}^2$ . Data was collected at a total of  $57 \times 57 = 3249$  discrete points on a square grid, where each point was separated by 2.22 cm in both the vertical and horizontal dimensions. At each of the 3249 points, co-polarization (HH and VV) data was collected at 201 frequencies between 2 and 3 GHz in a 5 MHz step with an Agilent network analyzer model ENA 5071B.

The scene being imaged was populated with one 5-drawer metal filing cabinet, one wooden desk, one chair, one desktop computer consisting of a CPU and monitor, one telephone, one 5-gallon jug of saline solution, one 1.22m-long pipe with a 5 cm diameter, three 15.24 cm trihedrals, and two 7.62 cm trihedrals, as shown in Fig. 2(b). The scene under surveillance is located within the investigation domain of  $D_S = [-1.83, 1.83]\text{m} \times [0, 1.778]\text{m} \times [0, 6.4]\text{m}$ . Since the width and height of targets of interest are important features for classification in TWRI applications, we perform a sparse reconstruction in the crossrange ( $x$ )-height ( $y$ ) domain for given a certain downrange ( $z$ ) location. We uniformly discretize the entire image into a 2-D square grid with an interval of 0.05 m in both crossrange and height.

In processing the experimental data, the following hyperparameters are used:  $a = b = c = d = 10^{-6}$ . The nonlinear functions are, respectively,  $e_i = 1/(1 + e^{4-\kappa_i})$  and  $f_i = e^{4-\kappa_i}/(1 + e^{4-\kappa_i})$ . The maximum number of iterations in the Gibbs sampling is 200, and the maximum marginal likelihood results in the last 20 samples are chosen as the estimate of  $\mathbf{w}$ . In addition, both HH and VV polarization

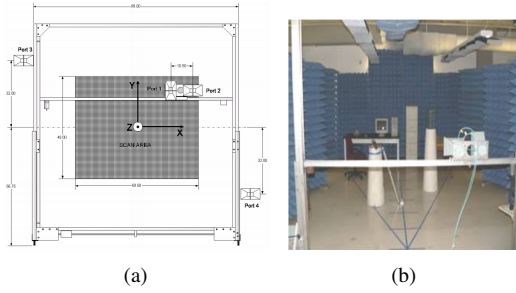


Fig. 2. Experiment antennas and scenarios. (a) Damaskos Field Probe Scanner Model 7X7Y with antennas. (b) Populated scene.

datasets are used, and only 25% randomly selected array positions and 20% randomly selected frequencies for each polarization are employed for scene reconstruction.

Fig. 3(a) shows the back-projected image in the  $x$ - $y$  domain at a downrange of 5.51 m (corresponding to the location of the metal filing cabinet) using all available data for the VV polarization. The filing cabinet is 1.5 m high and 0.6 m wide. It is easy to recognize the bright spot in Fig. 3(a) as the filing cabinet according to these features. The back-projected image corresponding to the reduced set of measurements is depicted in Fig. 3(b), which shows a degraded image of the filing cabinet with a much larger extent and cluttered background due to insufficient frequency and array position samples. Fig. 3(c) shows the sparse reconstruction result based on the method proposed in [5], which considers group sparsity across multiple polarization modes within the BCS framework. It is evident that the algorithm generates a low quality reconstruction result with many isolated and spurious pixels due to lack of consideration of the underlying target structure. On the other hand, the reconstructed scene obtained using the proposed algorithm, shown in Fig. 3(d), accurately locates the target. By exploiting the target clustering structure, it provides a highly concentrated image of the filing cabinet with relatively clear background. The acquired target features, including the height and width, closely match the true ones.

## V. CONCLUSION

We cast through-the-wall radar imaging as a sparse reconstruction problem to be effectively solved using emerging compressive sensing techniques. In particular, we jointly utilized the clustering sparsity of the targets due to their extended spatial occupancy and the group sparsity across multiple polarization modes for improved image reconstruction performance. We solved the resulting inverse scattering problem by using a generalized approach of the clustered multi-task Bayesian compressive sensing algorithm. Results based on real data collected in a laboratory environment demonstrated the effectiveness and superiority of the proposed approach.

## REFERENCES

- [1] M. G. Amin, *Through-the-Wall Radar Imaging*. CRC Press, 2010.
- [2] M. G. Amin, *Compressive Sensing for Urban Radars*. CRC Press, 2014.
- [3] M. Leigsnering, F. Ahmad, M. G. Amin, and A. M. Zoubir, "Compressive sensing based specular multipath exploitation for through-the-wall radar imaging," in *Proc. IEEE ICASSP*, Vancouver, Canada, May 2013.
- [4] Q. Wu, Y. D. Zhang, M. G. Amin, and F. Ahmad, "Through-the-wall radar imaging based on modified bayesian compressive sensing," in *Proc. IEEE China Summit and Int. Conf. Signal and Inform. Proc.*, Xi'an, China, July 2014.
- [5] A. Bouzerdoum, F. H. C. Tivive, and V. H. Tang, "Multi-polarization through-the-wall radar imaging using joint Bayesian compressed sensing," in *Proc. Int. Conf. Digital Sig. Proc.*, Hong Kong, China, Aug. 2014.
- [6] L. Jacob, G. Obozinski, and J. Vert, "Group Lasso with overlap and graph Lasso," in *Proc. Int. Conf. Machine Learning*, Montreal, Canada, Jun. 2009.
- [7] M. Yuan and Y. Lin, "Model selection and estimation in regression with grouped variables," *J. Royal Statist. Soc. Series B*, vol. 68, no. 1, pp. 49–67, 2006.
- [8] S. Ji, D. Dunson, and L. Carin, "Multitask compressive sampling," *IEEE Trans. Signal Proc.*, vol. 57, no. 1, pp. 92–106, 2009.
- [9] L. Poli, G. Oliveri, P. Rocca, and A. Massa, "Bayesian compressive sensing approaches for the reconstruction of two-dimensional sparse scatterers under TE illumination," *IEEE Trans. Geosci. Remote Sens.*, vol. 51, no. 5, pp. 2920–2936, 2013.
- [10] L. Poli, G. Oliveri, P. Rocca, and A. Massa, "MT-BCS-based microwave imaging approach through minimum-norm current expansion," *IEEE Trans. Ant. Propag.*, vol. 61, no. 9, pp. 4722–4732, 2013.
- [11] Q. Wu, Y. D. Zhang, M. G. Amin, and B. Himed, "Complex multitask Bayesian compressive sensing," in *Proc. IEEE ICASSP*, Florence, Italy, May 2014.
- [12] Q. Wu, Y. D. Zhang, M. G. Amin, and B. Himed, "Multi-static passive radar SAR imaging based on Bayesian compressive sensing," in *Proc. SPIE*, vol. 9109, Baltimore, MD, May 2014.
- [13] W. Deng, W. Yin, and Y. Zhang, "Group sparse optimization by alternating direction method," Rice Univ. Tech. Rep. TR11-06, 2011.
- [14] S. D. Babacan, S. Nakajima, and M. N. Do, "Bayesian group-sparse modeling and variational inference," *IEEE Trans. Signal Proc.*, vol. 62, no. 11, pp. 2906–2921, 2014.
- [15] L. Yu, H. Sun, J. P. Barbot, and G. Zheng, "Bayesian compressive sensing for cluster structured sparse signals," *Signal Proc.*, vol. 92, no. 1, pp. 259–269, 2012.
- [16] Q. Wu, Y. D. Zhang, M. G. Amin, and B. Himed, "Multi-task bayesian compressive sensing exploiting intra-task dependency," *IEEE Signal Proc. Lett.*, vol. 22, no. 4, pp. 430–434, 2015.
- [17] R. Solimene, F. Soldovieri, G. Prisco, and R. Pierri, "Three-dimensional through-wall imaging under ambiguous wall parameters," *IEEE Trans. Geosci. Remote Sens.*, vol. 47, no. 5, pp. 1310–1317, 2009.
- [18] W. Zhang, A. Hoorfar, C. Thajudeen, and F. Ahmad, "Full polarimetric beam-forming algorithm for through-the-wall radar imaging," *Radio Science*, vol. 46, no. RS0E16, pp. 1–17, 2011.
- [19] M. Bertero and P. Boccacci, *Introduction to Inverse Problems in Imaging*. Inst. Phys., 1998.
- [20] A. Gurbuz, J. McClellan, and W. Scott, "Compressive sensing for subsurface imaging using ground penetrating radar," *Signal Process.*, vol. 89, no. 10, pp. 1959–1972, 2009.

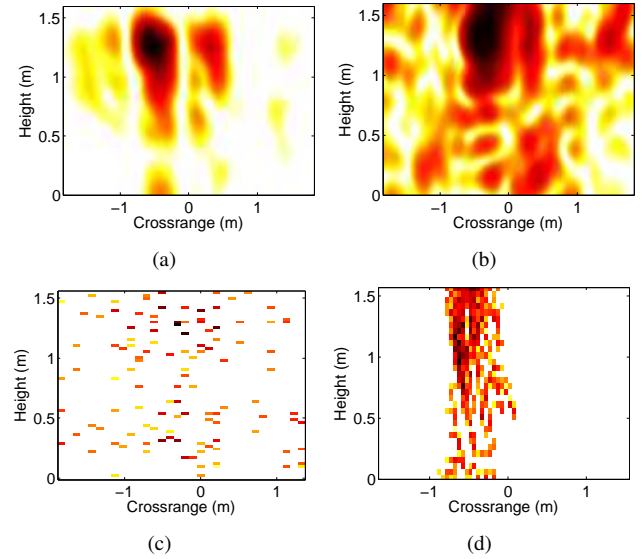


Fig. 3. (a) Back-projected image using full VV-polarized data. (b) Back-projected image using reduced VV-polarized data. (c) Sparse reconstruction result obtained with the method in [5] using reduced data with both VV and HH polarizations. (d) Sparse reconstruction result of the proposed method using reduced data with both VV and HH polarizations.